Synchronization of coupled biological oscillators under spatially heterogeneous environmental forcing

Andreas Bohn, Jordi García-Ojalvo

Synchronization of coupled biological oscillators under spatially heterogeneous environmental forcing

Andreas Bohn, Jordi García-Ojalvo

PII: S0022-5193(07)00469-9
DOI: doi:10.1016/j.jtbi.2007.09.036
Reference: YJTBI 4872

To appear in: *Journal of Theoretical Biology*

Received date: 16 February 2007
Revised date: 14 September 2007
Accepted date: 25 September 2007

Cite this article as: Andreas Bohn and Jordi García-Ojalvo, Synchronization of coupled biological oscillators under spatially heterogeneous environmental forcing, *Journal of Theoretical Biology* (2007), doi:10.1016/j.jtbi.2007.09.036

Synchronization of coupled biological oscillators under spatially heterogeneous environmental forcing

Andreas Bohn * and Jordi García-Ojalvo

Departament de Física i Enginyeria Nuclear, Universitat Politècnica de Catalunya, Colom 11, 08222 Terrassa / Barcelona, Spain

Abstract

Spatially heterogeneous intensities of environmental signals are common in nature, being caused, e.g., by rugged or curved surfaces leading to varying angles of incidence and intensities. In this work, we perform numerical studies of one-dimensional arrays of coupled phase oscillators driven by a periodic signal with spatially heterogeneous amplitude, considering both random and gradual amplitude distributions of the driving. We compare the effects of global and next-neighbor interactions, respectively, on the mutual and forced synchronization in the array. Weak global coupling leads to full mutual synchronization for all studied driving configurations. The degree of external synchronization follows a majority rule, depending on the number of externally entrained oscillators in the uncoupled case. The effects of next-neighbor coupling depend on the spatial distribution of the driving amplitude. For random distributions, local interactions show the same qualitative effects as global coupling. In contrast, for gradual distributions and large driving heterogeneities, next-neighbor coupling is detrimental to both mutual and external synchronization. We discuss these observations with respect to fundamental aspects of heterogeneity

and variability of dynamical systems, as well as the intercellular synchronization of circadian oscillators.

Key words: Synchronization, heterogeneity, phase oscillator, external field, circadian rhythm

1 Introduction

Periodic processes are at the heart of numerous dynamical phenomena in biological sciences, with time-scales ranging from milliseconds to years (Winfree, 2001; Strogatz, 2003; Moser et al., 2006). Many of these molecular and physiological rhythms are related to geophysical cycles like, e.g., the 24h-oscillation of day and night, giving rise to circadian rhythms and the corresponding biological timekeeping systems (Gillette and Sejnowski, 2005). In the past years, networks of multiple, interacting clocks have received increased attention in the field of chronobiology (Roenneberg and Merrow, 2003; Yamaguchi et al., 2003).

As circadian clocks are so-far known to be built on intracellular processes, multicellular tissues like, e.g. plant leaves, can be considered as multi-clock systems (Millar, 1998). Recent experiments and data analyses of in-vivo circadian rhythms in leaves of a higher plant showed that under weak periodic

* Corresponding author. Present address: Grupo de Biomatemática, Instituto de Tecnologia Química e Biológica, Universidade Nova de Lisboa, R Quinta Grande 6, 2780-156 Oeiras, Portugal. Tel +351 214 469 852, Fax +351 214 428 766.
Email addresses: abohn@itqb.unl.pt (Andreas Bohn),
jordi.garcia-ojalvo@upc.edu (Jordi García-Ojalvo).

light stimuli, the leaf is divided into clusters which are entrained to an external 24h oscillation of light intensity, while others remain unlocked, exhibiting free-running circadian oscillations (Rascher et al., 2001; Bohn, 2003). It was conjectured that these dynamics are caused by the heterogeneous distribution of light intensity throughout the leaf, caused by the curvature of the leaf surface in conjunction with the absence of interactions between different leaf regions due to high diffusion resistances in the leaf tissue. Derived from these findings, our work is motivated by the question whether coupling among the constituent elements of spatially extended systems under heterogeneous external forcing can simultaneously improve the mutual synchronization of the elements, as well as the degree of synchronization to the external forcing field.

This kind of question has already been addressed in the field of complex nonlinear systems. For example Hemming and Kapral (2000) have studied the formation of spatiotemporal patterns in oscillatory reaction-diffusion systems under periodic stimulation with spatially random amplitudes, detecting front roughening and spontaneous nucleation of target patterns. The present work features a less complex scenario, as we consider phase oscillators, a minimal model for periodic processes that has also been featured in a vast number of studies on complex dynamical systems (Tass, 1999; Winfree, 2001). In particular the Kuramoto model, which is made of mean-field (globally) coupled phase-oscillators, has provided deep analytical insight into the mechanisms of synchronization (Kuramoto, 1984; Acebrón et al., 2005). Our approach to assess the effects of heterogeneous environmental driving is based on a generalized version of this model that includes an additional external forcing field, as studied by Sakaguchi (1988) for the case of homogeneous forcing amplitudes and Arenas and Pérez Vicente (1994) for heterogeneous amplitudes with ran-

dom spatial distributions. These works reveal the conditions under which the coherence of the array, i.e. the mean-field amplitude, undergoes a transition from steady-state to oscillatory behavior. The effects of driving forces acting on arrays of coupled oscillators with heterogeneous phases have recently been depicted by Brandt et al. (2006), showing that intermediate phase disorder enhances network synchronization.

We extend those previous works by comparing i) the effects of global versus next-neighbour coupling, and ii) the influence of randomly distributed forcing amplitudes versus corresponding gradual patterns. We thus confront two extreme situations with respect to spatial scale, putting none or the most minimal spatial correlation possible (local coupling, random driving force amplitudes) against a system-wide space scale (global coupling, gradual driver patterns). In view of our motivation to connect recent spatiotemporal phenomena observed in experimental plant physiology with the extensive theoretical work in dynamical pattern formation, we restrict ourselves to these extreme cases. Both global and next-neighbour coupling have been intensively studied so far, and both can be depicted with biological meaning: global coupling with a quickly diffusing messenger, and local coupling with a substance with a very low diffusion constant with respect to the time-scale of the oscillator.

Our results confirm former findings that global coupling is more efficient in synchronizing non-identical oscillators than local interactions (Sakaguchi et al., 1987; Acebrón et al., 2005). A novel aspect surging from our studies is that the efficiency gap between both coupling types apparently depends on the spatial structure of the external forcing: a small spatial correlation of the external pattern provides synchronization properties similar to global coupling, while under gradual forcing patterns with large spatial correlation

lengths, local coupling might even elicit negative consequences for the degree of mutual and external synchronization.

This work is organized as follows: In Section 2 we introduce the mathematical framework, the observables used to describe spatiotemporal dynamics, and the choice of parameter values. The results of our simulations are presented in Section 3. We start by considering the case of uncoupled arrays, followed by combinations of each of the coupling types and external driving patterns for strong coupling and a discussion of the system dynamics as a continuous function of increasing coupling strength. We add results for simulations with intermediate noise strength and with an alternative distribution of natural frequencies. In Section 4 we discuss the results, both with respect to the intercellular coupling of circadian rhythms, as well as general aspects of spatio-temporal dynamics and synchronization under heterogeneous external forces.

2 Modeling and analysis methods

2.1 Systems of coupled phase oscillators

Our numerical studies are based on the Kuramoto model, describing the temporal evolution of phases φ_i in a one-dimensional array of $i = 1, ..., N$ globally coupled phase oscillators with natural frequencies ω_i, and coupling strength K. Given an additional term for a periodic external field with amplitudes ε_i, phase Φ and frequency $\dot{\Phi} = \omega_e$, one writes (Sakaguchi, 1988)

$$\dot{\varphi}_i = \omega_i + \frac{K}{N}\sum_{j=1}^{N}\sin(\varphi_j - \varphi_i) + \varepsilon_i \sin(\Phi - \varphi_i). \quad (1)$$

Transforming to the rotating frame of the external driver and substituting the phase differences $\phi_i(t) = \varphi(t) - \Phi(t)$ and natural frequency mismatches $\nu_i = \omega_i - \omega_e$, we obtain an expression for the evolution of the phase differences between each individual oscillator and the external driver

$$\dot{\phi}_i = \nu_i + \frac{K}{N}\sum_{j=1}^{N}\sin(\phi_j - \phi_i) - \varepsilon_i \sin\phi_i + \xi_i(t)\,, \tag{2}$$

where stochastic effects are represented by a white, Gaussian noise with zero mean and correlation $< \xi_i(t)\xi_j(t') >= 2D\delta_{ij}\delta(t-t')$.

We compare the globally coupled system (2) with a system where the interactions involve only the next neighbors of each oscillator, by modifying the coupling term in (2) in order to obtain

$$\dot{\phi}_i = \nu_i + \frac{K}{3}\sum_{j=i-1}^{i+1}\sin(\phi_j - \phi_i) - \varepsilon_i \sin\phi_i + \xi_i(t). \tag{3}$$

We integrate these equations with a second-order Heun scheme for $N = 1000$ oscillators, with initial values $\phi_i(0)$ being randomly distributed in $[0.8, 1.2]$ and time steps $\delta t = 0.1$. Each realization extends over 3000 timesteps, discarding the first 1000 steps as transient. In the case of next-neighbour coupling, periodic boundary conditions are used. Running the simulations for a smaller array with $N = 100$ yields the same qualitative results (data not shown).

2.2 Spatiotemporal data analysis

In the following, we define the observables used to characterize the state of synchronization and the spatiotemporal dynamics of the array. One part of them is based on the distribution $P(\Omega_i)$ of the real frequencies Ω_i, which

are defined as the average increase of ϕ_i per unit of time calculated over $m = 1, \ldots, M-1$ timesteps.

$$\Omega_i = \frac{1}{M} \sum_{m=1}^{M-1} \frac{\phi_i(t_{m+1}) - \phi_i(t_m)}{\delta t}, \tag{4}$$

where $\delta t = t_{m+1} - t_m$ for all m. From $P(\Omega_i)$ we compute the spatially averaged frequency $\overline{\Omega}$, as well as the spatial standard deviation $\sigma(\Omega_i)$, the latter defining the degree of internal frequency disorder, which is inversely proportional to the degree of mutual entrainment.

The *degree of forced entrainment*, η, is defined as the proportion of oscillators with $\Omega = 0$, i.e. no average real-frequency mismatch with the external driver, reading

$$\eta = P(\Omega_i = 0). \tag{5}$$

As Ω is a temporally averaged frequency, it provides a relatively weak measure of synchronization, in terms of frequency locking. A further, more rigorous quantity for mutual entrainment, implicitly expressing phase order is the mean-field amplitude (Kuramoto, 1984)

$$R = \frac{\sqrt{\left(\sum_{i=1}^{N} \sin\phi_i\right)^2 + \left(\sum_{i=1}^{N} \cos\phi_i\right)^2}}{N}. \tag{6}$$

For a given set of parameters, we compute its temporal average $\widehat{R}$ and its amplitude $\Delta R = \max_t(R) - \min_t(R)$. We consider the array to be in full simultaneous, i.e. mutual and external, synchronization, when the conditions

$$\eta > \eta_{thresh} = 0.99,\ \widehat{R} > \widehat{R}_{thresh} = 0.98,\ \Delta R < \Delta R_{thresh} = 0.001 \tag{7}$$

are simultaneously fulfilled. Both η_{thresh} and ΔR_{thresh} are chose arbitrarily, while on a 24h-scale $\widehat{R}_{thresh} = 0.98$ corresponds to an average phase spread of about $\pm$1.2h, which is similar to the spread in natural periods of circadian oscillations (see below). As the results section will show, in most cases $\widehat{R}_{thresh}$ is the limiting factor for simultaneously achieving both external and internal synchronization. Lowering $\widehat{R}_{thresh}$ would increase the proportion of the parameter space in which full synchronization is observed.

2.3 Spatial distribution of natural frequencies and forcing amplitudes

We assume both the natural frequencies ν_i and the driving amplitudes ε_i to be uniformly distributed over the intervals $[\overline{\nu} - \Delta\nu, \overline{\nu} + \Delta\nu]$ and $[\overline{\varepsilon} - \Delta\varepsilon, \overline{\varepsilon} + \Delta\varepsilon]$, respectively, given the center values $\overline{\nu}$ and $\overline{\varepsilon}$, and variabilities $\Delta\nu$ and $\Delta\varepsilon$. In all simulations, the ν_i are distributed in a random fashion over the grid. For ε_i, in addition to the random distribution, we also investigate gradual distributions (Fig. 1). With periodic bounds given, we need to maintain steady parameter values at the edges of the system. Therefore, we use the expression

$$\varepsilon_i = \overline{\varepsilon} + \Delta\varepsilon \left(1 - 2 \cdot \frac{|2i - N - 1|}{N - 1}\right), \tag{8}$$

to compute gradual patterns of ε_i, which rise from $\overline{\varepsilon} - \Delta\varepsilon$ at $i = 1$ to $\overline{\varepsilon} + \Delta\varepsilon$ at $i = (N-1)/2$, and decline back to $\overline{\varepsilon} - \Delta\varepsilon$ at $i = N$. As each $\varepsilon_i \in [\overline{\varepsilon} - \Delta\varepsilon, \overline{\varepsilon} + \Delta\varepsilon]$ appears twice, the corresponding random patterns of ε_i are computed as two independent uniform random distributions for $i \leq N/2$, and $i > N/2$, respectively.

2.4 Parameter values

As this work is inspired by circadian rhythms and their synchronization to signals with 24-hour period, we are interested in the 1:1 synchronization with the environment, and therefore chose a range of small values for ν_i. Our default parameters are $\overline{\nu} = 0.02$, and $\Delta\nu = 0.05$. Assuming that $\omega_e = 1$ corresponds to a period $\tau = 24$ h, this parameter configuration corresponds to circadian oscillations of 23.5 ± 1.2 h (Gonze et al., 2005).

Figure 2 (left) depicts the resonance diagram of a single phase oscillator, indicating the 1:1 locking zone determined by (Winfree, 2001)

$$\varepsilon \geq \nu \tag{9}$$

The overlaid rectangle is defined by the distributions of ν_i and ε_i. For the uncoupled case $K = 0$, one may recognize some structures in the forcing-parameter space $\Delta\varepsilon$ vs. $\overline{\varepsilon}$, Fig. 2 (right), by purely geometrical arguments derived from Fig. 2 (left). For instance, one may deduce that the synchronization of the array should be largely dominated by the external driver if the rectangle is fully contained in the locking zone. For $\overline{\nu} > 0$ this is the case if the lower right corner of the rectangle $(\overline{\nu} + \Delta\nu, \overline{\varepsilon} - \Delta\varepsilon)$ is inside the locking zone, i.e. $\overline{\varepsilon} - \Delta\varepsilon \geq \overline{\nu} + \Delta\nu$. Together with Eq. (9) this corresponds to the section of the forcing-parameter space given by

$$\Delta\varepsilon \leq \overline{\varepsilon} - \overline{\nu} - \Delta\nu. \tag{10}$$

Furthermore we require the driving amplitude to be positive for all oscillators, i.e. $\overline{\varepsilon} - \Delta\varepsilon > 0$, thus excluding the region

$$\Delta\varepsilon > \overline{\varepsilon} \tag{11}$$

from consideration. As will be seen in the following chapters, expressions (10) and (11), which are fully determined by the choice of $\overline{\nu}$ and $\Delta\nu$, delimit the area of the forcing-parameter space where the most apparent differences between the considered coupling types and spatial driving patterns are evidenced. To focus our attention on this section of the parameter space, we choose $\overline{\varepsilon}, \Delta\varepsilon \in [0, 0.2]$, without limitation of the general validity of the results.

2.5 Symbol survey

All used symbols are gathered and explained in Table 1.

3 Results

3.1 Uncoupled oscillators, K=0

We start our analysis by monitoring the observables of spatiotemporal dynamics defined in the previous section for the uncoupled case, $K = 0$, and in the absence of noise, $D = 0$ [Fig. 3(a-e)]. Two principal areas dominate the forcing-parameter space. First, the lower left corner ($\overline{\varepsilon}, \Delta\varepsilon \approx 0$), where one finds the maximum values of $\overline{\Omega}$, $\sigma(\Omega_i)$, and ΔR (panels a,b,e), and minimum values of η, and $\widehat{R}$ (c,d). Here, due to the spread of natural frequencies $\Delta\nu$ and weak driving forces, the array exhibits low mutual and external synchro-

nization. This behavior extends along the line $\Delta\varepsilon = \overline{\varepsilon}$, where $\min_i(\varepsilon_i) = 0$, but is less pronounced as $\overline{\varepsilon}$ becomes much larger than zero.

The second principal area is the sector in the lower right corner delimited by (10), where all oscillators are mutually and externally entrained, as is manifested by $\overline{\Omega}$, $\sigma(\Omega_i)$, and $\Delta R \approx 0$, as well as η, and $\widehat{R} \approx 1$. Inspecting the spatio-temporal dynamics in the array for this parameter region, one observes temporally stationary relative phases ϕ_i, exhibiting a spatially heterogeneous pattern due to the randomly distributed natural frequency mismatches ν_i (data not shown). The subspace of temporal constancy of the mean-field ($\Delta R = 0$) is delimited by the gray solid line in Fig. 3(e), and roughly coincides with Eq. (10), while $\eta > \eta_{\mathrm{thresh}}$ holds for an even larger area of the parameter space [gray solid line in Fig. 3(c)]. Due to the spatial heterogeneity of ϕ_i, however, the condition $\widehat{R} > R_{\mathrm{thresh}}$ is fulfilled only in a smaller section, here to be found in the very lower right corner of Fig. 3(d) (gray line).

3.2 Coupled arrays, K=2

To assess the effect of coupling, we first consider $K = 2$, as for this value the patterns in the forcing-parameter space are stationary with respect to further increases of K.

Random driving - global coupling

The first scenario we investigate is the combination of randomly distributed ε with global coupling, following the model described by Eqs. (2). The behavior of this system is displayed in Figs. 3(f-k). Again, for the moment, the

noise intensity is assumed zero, $D = 0$. There is a clear difference between the measures based on the real frequencies Ω_i, panels (f)-(h), and the mean-field statistics $\widehat{R}, \Delta R$, panels (j) and (k). While the latter clearly indicate full mutual synchronization in the entire parameter space, the former reveals a bisection at a value of $\overline{\varepsilon} = \overline{\nu} = 0.02$. For $\overline{\varepsilon} > \overline{\nu}$ the system is fully entrained to the external driver, while for $\overline{\varepsilon} < \overline{\nu}$, $\eta = 0$ (h) and $\overline{\Omega} > 0$ (f). The frequency disorder $\sigma(\Omega_i)$ shows non-zero values in a transition zone around $\overline{\varepsilon} \approx \overline{\nu}$.

Figure 4(a) depicts the spatio-temporal dynamics of the mutually but not externally synchronized array, which is observed for $(\overline{\varepsilon}, \Delta\varepsilon) = (0.015, 0.01)$. The location of this point is marked with a cross in Figs. 3(f-k). Inspection of the spatiotemporal dynamics confirms the full mutual synchronization, while the periodic dynamics of the entire array exhibits lack of synchronization with the external driver. This is shown in Fig. 4(d), which depicts the distribution of actual frequencies, $P(\Omega_i)$, versus the coupling strength K. It is evidenced that the global interaction forces the distribution of natural frequencies into synchrony for fairly low values of K, such that the array locks to a common frequency $\overline{\Omega}$ different from the driving frequency, with $0 < \overline{\Omega} < \overline{\nu} = 0.02$.

Global coupling thus provides mutual synchronization for all combinations of $\overline{\varepsilon}$ and $\Delta\varepsilon$. However, the common system frequency and hence η depend on the configuration of ε. The line $\overline{\varepsilon} = \overline{\nu}$ in Fig. 3(h), which marks the transition from $\overline{\Omega} > 0$ to $\overline{\Omega} = 0$ corresponds in Fig. 3(c) (i.e. for $K > 0$), to $\eta = 0.5$. In other words, global coupling leads to full external synchronization of the entire array if the majority, i.e. more than half, of the oscillators are already synchronized with the external driver in the absence of inter-oscillator coupling. In the geometrical terms of Fig. 2, global coupling yields full external synchronization if the center of mass of the (ν, ε) rectangle lies with the resonance zone of the

single oscillator.

Random driving - local coupling

A bisection of parameter space is also evident for the locally coupled system (3) under random forcing amplitudes [Figs. 3(l-p)]. However, a detailed examination yields a number of differences with respect to the case of global coupling.

First of all, both mutual and external entrainment is observed for $\overline{\varepsilon} \geq 0.03$, which in terms of the used parameters is equivalent to $\overline{\varepsilon} \geq \Delta\nu - \overline{\nu}$. Hence, the bisection line is shifted to higher average driving forces. Also this line is not completely straight as in the case of global coupling. The second major difference is that for $\overline{\varepsilon} < \Delta\nu - \overline{\nu}$ no mutual entrainment is achieved, as is manifested mainly by the frequency disorder $\sigma(\Omega_i) > 0$ and $\Delta R \gg 0$. Roughly speaking, for the given scenario at $K = 2$, we observe either mutual and external synchronization together, or no synchronization at all.

The spatio-temporal dynamics in the non-synchronization regime, with $(\overline{\varepsilon}, \Delta\varepsilon)$ indicated by the gray cross in Figs. 3(l-p), shows that the random combination of ν_i and ε_i, plus the effect of coupling, leads to phase waves running through the array, leading to low values of both $\sigma(\Omega_i)$ and η (Fig. 4b). Hence, only if the influence of the external force is sufficiently dominant, both heterogeneities are overcome in order to yield low $\sigma(\Omega_i)$ and high η. The dependence of the frequency distribution $P(\Omega_i)$ on K, displayed in Fig. 4(e), shows that the transient behavior spreads over an interval of K $(0 < K < 0.5)$ larger than in the case of global coupling. For large enough K, the stationary situation consists of oscillations with a common Ω, but low $\widehat{R}$ and high ΔR, as the

local coupling does not compensate the randomness to the extent of providing in-phase oscillations throughout the array.

Gradual driving - local coupling

For the case of global coupling, the system's behavior is invariant to the spatial structure of the driving. We hence consider the scenario of a gradual driving only for local coupling [Fig. 3(q-u)]. Here, the structure in the $(\overline{\varepsilon}, \Delta\varepsilon)$-space clearly differs from the two aforementioned scenarios. A large area without external locking extends between the lines delimited by Eq. (11) and

$$\Delta\varepsilon \leq \overline{\varepsilon} + \overline{\nu} - \Delta\nu. \tag{12}$$

The latter apparently approximates the maximum extension of the area of the parameter space where the conditions (7) are fulfilled (gray lines in Figs. 3(s-u)). The geometrical correspondence of expression (12) is the inclusion of the lower left corner of the distribution rectangle into the locking zone [Fig. 2(left)]. In terms of the probability distribution of Ω_i for $K = 0$, this situation corresponds to the situation where $\Omega_i \geq 0$, i.e. the array consists of either externally locked oscillators ($\Omega_i = 0$) or oscillators whose real frequencies are higher than the external driver ($\Omega_i > 0$). Hence, with the gradual driving pattern, local coupling only leads to full external synchronization, if there are no $\Omega_i < 0$ in the uncoupled case $K = 0$.

The spatio-temporal dynamics of an array with $\overline{\varepsilon} = 0.06, \Delta\varepsilon = 0.05$ is depicted in Fig. 4(c). The space is divided in two sections: first, the center region of intermediate oscillator indices, featuring large ε, yielding a sub-array that is phase locked to the external driver, as is manifested by temporally constant Ω_i.

The non-locked regions at the margins of the array show running phase waves, resembling the dynamics of Fig. 4(b). In the probability distribution $P(\Omega_i)$, shown in Fig. 4(f) these dynamics are reflected by a stationary bimodality for large enough K, with peaks at $\Omega = 0$ and $\Omega < \overline{\nu} = 0.02$.

3.3 Increasing coupling strength, K=0...2

In Fig. 5 we quantify the effects of coupling strengths K in the range [0..2] by measuring the proportion of the $(\overline{\varepsilon}, \Delta\varepsilon)$-space, where η, $\widehat{R}$ and ΔR are above their respective thresholds (7). The top row corresponds to the three cases with $K > 2$ in Fig. 3(f-u). Notice the smaller scale of the x-axis for the case of global coupling (left column), corresponding to the reduced transient zone caused by the high synchronization efficiency of global coupling [Fig. 5(a)]. Starting from $K = 0$ the smallest area above threshold, which limits the full-locking zone (indicated by the bold solid line) is defined by $\widehat{R}$ (triangular symbols), up to $K = 0.15$, where η (diamond symbols) becomes and remains the limiting quantifier for large K. In that case, while the mean-field related measures are above threshold in the entire parameter space, η occupies about 95% of its total area [cf. Figs. 3(h-k)].

The case of random driving and local coupling shown in Fig. 5(b) confirms the results plotted in Figs. 3(n-p), in the sense that full external locking is observed in a somewhat smaller area than with global coupling, and it takes higher values of K to reach the maximum area, which is about 90%. The limiting factor for full entrainment area is the temporal average of the mean-field $\widehat{R}$.

The latter also holds true for the scenario of gradual forcing with local coupling [Fig. 5(c)]. As stated in the previous section, the above-threshold areas for this scenario are considerably lower, reaching a maximum coverage of about 60% of the parameter space. Deviations from a monotonous increase of the observables with K [e.g. η in Fig. 5(c)] are due to the loss of some above-threshold areas at the borderlines, which is caused by the implicit randomness and averaging over a limited number of realizations (data not shown).

3.4 Noise effects

In order to study the effects of noise, we scanned the driving-parameter space in the same fashion as before, for non-zero noise intensities. The bottom row of Fig. 5 shows the above-threshold proportions for the noisy system. In all scenarios, the least affected observable is η, as is to be expected for a temporally averaged quantity. For global coupling, the principal effect is to shift the increase of the area with $\widehat{R} > \widehat{R}_{thresh}$ to higher K values (Fig. 5d). Nevertheless, a situation identical to the deterministic case is fully recovered at about $K = 0.4$. For local coupling, noise has a significant impact on the mean-field properties, as is observed by clearly diminished proportions of area above threshold in comparison to the deterministic case [Figs. 5(e,f)]. Different from this, however, for high values of K, the limit for full forced entrainment is given by ΔR (square symbol), not $\widehat{R}$ (triangles). For local coupling, we compare the structures of the full-locking zones in the $(\overline{\varepsilon}, \Delta\varepsilon)$-space for both the deterministic and stochastic cases in Fig. 6. It is clear that noise leads to a shrinking of the above-threshold area for both spatial driving patterns, but does not introduce any qualitative changes of the structure of the zones detected in the

deterministic case (solid lines, correspond to Fig. 3).

The fact that global coupling is more efficient in achieving mutual and forced synchronization also under the influence of noise nourishes the evidence that the attaining population synchrony despite environmental heterogeneity might better be achieved with long-range interactions given by mean-field coupling.

3.5 One-sided natural frequency distribution

In a final set of simulations we investigated a one-sided distribution of natural frequencies, i.e. $\nu_i > 0$ for all oscillators, therefore choosing $\overline{\nu} = 0.1$ and maintaining $\Delta\nu = 0.05$ as before. In Fig. 7, we show the driving-parameter spaces for the four scenarios of Fig. 3, indicating the zones of simultaneous full external and mutual entrainment by the solid line. The cases in panels (a)-(c) clarify that the shape of the locking zones is congruent with the case of $\overline{\nu} = 0.02$, and thus show that the principal structure of the parameter space is not dependent on the particular choice of parameters for ν_i. In particular, global coupling again follows the majority rule of achieving $\eta = 1$ for $\overline{\varepsilon} > \overline{\nu}$ [Fig. 7(b)]. In the case of gradual driving and local coupling [Fig. 7(d)], the limits are close to the line

$$\Delta\varepsilon = \overline{\nu} + \overline{\varepsilon}, \tag{13}$$

corresponding to a location of the distribution rectangle in Fig. 2(left), where the point $(\overline{\nu},\, \overline{\varepsilon} - \Delta\varepsilon)$ enters the single-oscillator locking-zone. This implies that local coupling under a gradual driver pattern only leads to both mutual and external entrainment, if the the uncoupled array ($K = 0$) is exclusively composed of oscillators with $\Omega_i = 0$ or $\Omega_i \geq \overline{\nu}$ but does not contain systems

with $\Omega_i < \overline{\nu}$.

The apparent relation between the passage of given points of the distribution rectangle into the single-oscillator locking zone, and the onset of synchronization of the entire array, warrants a deeper, analytical and more detailed study of heterogeneously driven arrays of phase-oscillators with local coupling. Being beyond the scope of the present paper, this may be pursued in a future work.

4 Discussion

We have numerically investigated the mutual and forced synchronization of one-dimensional arrays of phase oscillators under the influence of an external periodic driver with heterogeneous forcing amplitudes, comparing the effects of global (mean-field) vs. local (next-neighbor) coupling for both random as well as gradual distributions of the external driver strength. The results of our work show that weak global coupling generally leads to full mutual synchronization of the array, with the resulting frequency being in between the central natural frequency $\overline{\nu}$ and the external frequency (Fig. 4a+d). Forced synchronization occurs for situations whenever more than half of the oscillators are phase-locked to the external driver in the absence of inter-oscillator coupling (Fig. 3f-k). Negative effects of intermediate noise levels on the synchronization can be fully compensated by moderately increasing the coupling strength (Fig. 5d). As expected, local coupling gives rise to much more complex dynamics, showing the co-existence of locked and unlocked zones in the array, together with running phase waves which emerge from the random distribution of natural frequencies and pattern of the external driver (Fig. 4c+f). It also

shows less efficiency in achieving mutual and forced synchronization, leading to smaller areas in the driving-parameter space with full internal and external synchronization, and a larger reduction of the degree of synchronization by noise (Fig. 5b,c,e,f). An interesting feature is the fact that this synchronizing efficiency also depends on the spatial structure of the external driver, with random driving patterns yielding results close to the case of global coupling, while the impact by large-scale gradual driving patterns implies a significantly diminished capability of achieving synchronization through next-neighbor interactions. As we discuss in the following, these results may contribute to the further understanding of intercellular coupling of biological rhythms, as well as the general effects of variability in non-linear dynamical systems.

Intercellular coupling of circadian clocks

Our work departed from results obtained from the quantitative analyses of circadian rhythms in leaves of a higher plant (Bohn, 2003). There, the coexistence of synchronized and non-synchronized patches in the leaves was related to the absence of intercellular coupling, which is caused by a very low intercellular CO_2 conductance, resulting from the small intercellular airspace in the succulent model plant *Kalanchoë daigremontiana* (Rascher et al., 2001). For circadian oscillations in plants, global coupling may be considered as a minimal model of high CO_2 conductance, as differences in CO_2 concentration may level out in the entire tissue on a much faster time-scale than 24h. Correspondingly, low conductance may be associated with next-neighbour coupling, which is in concordance with the simulation results (phase waves, synchronization clusters) and the experimental facts observed by Rascher et al. (2001).

The question, whether circadian rhythms in plants are coupled across cell boundaries is thus far undecided. In spite of the evidence for CO_2-mediated metabolic interactions between neighboring rhythmic patches in plant leaves (Duarte et al., 2005), and combined modeling and experimental work suggesting coupling to be important for the emergence of circadian rhythmicity in plant seedlings (Fukuda et al., 2004), other experimental results stress the functional independence of circadian clocks across cell boundaries (Thain et al., 2000). Together with our results one may thus conjecture that the most successful strategies to achieve robust synchronization to a heterogeneous environment are either by a high plasticity of cellular clocks, allowing synchronization in a large range of environmental conditions, or, in the case of existing cell-cell interaction, a highly diffusive coupling agent that transmits information throughout the array on a time-scale faster than 24h. Chlorophyll fluorescence has become a valuable tool to assess the spatio-temporal dynamics of metabolic processes in plant leaves in a fluctuating environment (Rascher and Lüttge, 2002). Periodic driving of leaf photosynthesis has thus far been performed on a time-scale of seconds (Nedbal and Brezina, 2002). If transferred to the 24h-scale, together with a deliberate manipulation of the spatial structure of light incidence, this technique could give access to imporant dynamical parameters such as the frequency distribution in the leaf, spatial correlation lengthes and the signal-to-noise ratio of the oscillations under spatially heterogeneous forcing. With plant leaves appropriately prepared at the tissue or cellular level, putative cell-cell coupling agents and their spatial motility could be detected in this fashion.

Outside the plant kingdom, numerous examples and models for intercellular coupling of circadian clocks support the mean-field mechanism. For example,

the synchronization of circadian oscillations of the unicellular algae *Gonyaulax polyhedra* was shown to be communicated by the intercellular medium (Broda et al., 1985). For animal clocks, it was suggested that the coupling of individual neurons in the suprachiasmatic nucleus is partly provided by the secretion of neurotransmitters into the intercellular space (Shirakawa et al., 2001). Accordingly, the model by Gonze et al. (2005) features global coupling and underlines its effectiveness. For the insect clock in *Drosophila*, a globally coupled model was put forward by Ueda et al. (2002). Our work adds to these evidences by showing that even by adding a common and realistic environment-bourne heterogeneity on top of the intrinsic variability due to the spread of natural frequencies of circadian clocks, global coupling proves to be a robust mechanism to provide system-wide mutual and forced synchronization. These results could support future experimental work on the mechanisms of cell-cell coupling of circadian clocks, by concentrating the search for suitable coupling agents towards those candidates that exhibit a sufficiently high conductivity in the intercellular medium.

The generality of the Kuramoto model would allow to extrapolate these conclusions to spatially heterogeneous signals and oscillations on any time and space-scale. In fact, the influence of combined spatial and temporal environmental heterogeneities plays an important role in theoretical ecology and evolution (Dieckmann et al., 1999). Even though the intrinsic dynamics of the featured reaction-diffusion models are generally not oscillatory, it is interesting to notice that also for other generic models of spatiotemporal dynamics, temporal heterogeneity in combination with spatial disorder favors high dispersion rates (Hutson et al., 2001).

Non-linear dynamics of heterogeneously forced systems

Adding to the ongoing work in mathematical and theoretical biology, the study of the effects of variability on spatio-temporal pattern formation has recently become a very active field of research in the physics of non-linear dynamical systems (Sendiña Nadal et al., 1998; Zhou et al., 2001; Glatt et al., 2006). From such a theoretical point of view, our work exposes extreme situations concerning the space scales of the external signal and the coupling. The random driving pattern, as well as the next-neighbor coupling give examples of the absence of spatial correlations, while the gradual pattern, and the global coupling have correlation lengths in the same order of magnitude of the total array extension. Our results suggest that in order to yield optimal adaption and synchronization to a heterogeneous environment through system-inherent interactions, the spatial scale of the internal interactions should be equal or larger than the scale of the external heterogeneity. Future work in this field should thus investigate the synchronization properties for external patterns and internal interactions by increasing their spatial ranges in a continuous fashion.

In our work, we address a current problem in plant biology with the mathematically most simple model possible and expose it to four well defined scenarios of external driving and coupling structure. The results of this work can be given realistic biological meaning, and at the same time could serve as a point of departure for future studies in complex nonlinear dynamics. We suggest four extensions of our model, which should lead to new insights to heterogeneously driven networks of oscillators: i) the spatial ranges of both coupling and external driving should be changed in a continuous fashion, in order to verify the hypothesis that full synchronization can be achieved whenever the coupling

scale is larger than the environmental space scale. ii) two-dimensional networks of coupled should be considered. Our results can be most easily transferred to 2D, by considering heterogeneities with radial symmetry. Running phase-waves like in Fig. 4 would then translate to target patterns. For anisotropic geometries we would expect scenarios of target patterns and complex phase-front propagation (Hemming and Kapral, 2000). According to Sakaguchi et al. (1987) achievement of full synchronization is easier in dimensions larger than one. In the long term, the relation of topology and synchronization as addressed by Arenas et al. (2006) should also be investigated under heterogeneous external driving. iii) The external signal should be modeled in a more realistic fashion, e.g. using a noisy external driver. As Zhou and Kurths (2002) point out, an intermediate level of such global noise, corresponding to random fluctuations on a time-scale faster than 24h, can enhance the phase synchronization of the array. iv) Finally the uniform distributions featured here could be substituted by more realistic, e.g. Gaussian, distributions. Earlier work by Arenas and Pérez Vicente (1994) showed that different distributions of, e.g. natural frequencies, do not yield different effects, as long as the distribution is unimodal, and symmetric around the mean value, which applies to both the uniform and the normal distribution. One might expect the strongest effects for the case of local coupling and random driving, as either natural frequencies or driver strengthes from the tail of the normal distribution might yield large perturbation, which would require significantly higher coupling strengthes to achieve synchronization. Qualitatively different effects might be expected from more complex assymmetric or multimodal distributions.

Acknowledgments

This work was supported by the European Commission under the project HPC-Europa (RII3-CT-2003-506079) at the European Centre for Parallelism of Barcelona (CEPBA). A.B. received financial support by the Fundação para a Ciência e a Tecnologia (Portugal), through fellowship SFRH/BPD/25967/2005. J.G.O. acknowledges financial support from the Ministerio de Educación y Ciencia (Spain) and FEDER (project FIS2006-11452), and from the Generalitat de Catalunya.

References

Acebrón, J. A., Bonilla, L. L., Pérez Vicente, C. J., Ritort, F., Spigler, R., 2005. The Kuramoto model: A simple paradigm for synchronization phenomena. Rev Mod Phys 77, 137–185.

Arenas, A., Pérez Vicente, C. J., 1994. Exact long-term behaviour of a network of phase oscillators under random fields. Phys Rev E 50, 949–956.

Arenas, A., Díaz Guilera, A., Pérez Vicente, C. J., 2006. Synchronization processes in complex networks. Physica D 224: 27-34.

Bohn, A., 2003. Analysis and simulation of multi-oscillator systems in a crassulacean acid metabolism plant. Ph.D. thesis, Dept of Physics, Darmstadt University of Technology, Germany.
URL `http://elib.tu-darmstadt.de/diss/000367`

Brandt, S. F., Dellen, B. K., Wessel, R., 2006. Synchronization form disordered driving forces in arrays of coupled oscillators. Phys Rev Lett 96, 034104.

Broda, H., Brugge, D., Honma, K., Hastings, J. W., 1985. Circadian communication between unicells? Cell Biophys 8, 47–67.

Dieckmann, U., O'Hara, B., Weisser, W., 1999. The evolutionary ecology of dispersal. Trends Ecol Evol 14, 88–90.

Duarte, H. M., Jakovljevic, I., Kaiser, F., Lüttge, U., 2005. Lateral diffusion of CO_2 in leaves of the Crassulacean acid metabolism plant Kalanchoë daigremontiana Hamet et Perrier. Planta 220, 809–816.

Fukuda, H., Kodama, J., Kai, S., 2004. Circadian rhythm formation in plant seedling: Global synchronization and bifurcation as a coupled nonlinear oscillator system. Biosystems 77, 41–46.

Gillette, M. U., Sejnowski, T. J., 2005. Biological clocks coordenately keep life on time. Science 309, 1196–1198.

Glatt, E., Gassel, M., Kaiser, F., 2006. Variability-induced transition in a net of neural elements: From oscillatory to excitable behavior. Phys Rev E 73, 066230.

Gonze, D., Bernard, S., Waltermann, C., Kramer, A., Herzel, H., 2005. Spontaneous synchronization of coupled circadian oscillators. Biophys J 89, 120–129.

Hemming, C.J., Kapral, R. 2000. Resonantly forced inhomogeneous reaction-diffusion systems. Chaos 10, 720-730.

Hutson, V., Mischaikov, K., Polácik, P., 2001. The evolution of dispersal rates in a heterogeneous time-periodic environment. J Math Biol 43, 501–533.

Kuramoto, Y., 1984. Chemical Oscillations, Waves and Turbulence. Springer, Berlin, Germany.

Millar, A. J., 1998. Biological Rhythms and Photoperiodism in Plants. Bios Scientific, Oxford, UK, Ch. The Cellular Organization of Circadian Rhythms in Plants: Not One But Many Clocks., pp. 51–68.

Moser, M., Frühwirt, M., Penter, R., Winkler, R., 2006. Why life oscillates - from a topological towards a functional chronobiology. Cancer Causes Control 17, 591–599.

Nedbal, L. and Brezina, V. 2003. Complex metabolic oscillations in plants forced by harmonic irradiance. Biophys J 83: 2180-2189.

Rascher, U., Hütt, M. T., Siebke, K., Osmond, C. B., Beck, F., Lüttge, U., 2001. Spatiotemporal variation of metabolism in a plant circadian rhythm: The biological clock as an assembly of coupled individual oscillators. Proc Natl Acad Sci USA 98, 11801–11805.

Rascher, U. and Lüttge, U. 2002. High-resolution chlorophyll fluorescence imaging serves as a non-invasive indicator to monitor the spatio-temporal variations of metabolism during the day-night cycle and during the endoge-

nous rhythm in continuous light in the CAM plant Kalanchoe daigremontiana. Plant Biol 4: 671-681.

Roenneberg, T. and Merrow, M. 2003. The Network of Time: Understanding the Molecular Circadian System. Curr Biol 13, R198-R207.

Sakaguchi, H., 1988. Cooperative phenomena in coupled oscillator systems under external fields. Prog Theor Phys 79, 39–46.

Sakaguchi, H., Shinomoto, S., Kuramoto, Y., 1987. Local and global self-entrainments in oscillator lattices. Prog Theor Phys 77, 1005–1010.

Sendiña Nadal, I., Muñuzuri, A. P., Vives, D., Pérez-Muñuzuri, V., Casademunt, J., Ramírez-Piscina, L., Sancho, J. M., Sagués, F., Jun 1998. Wave propagation in a medium with disordered excitability. Phys. Rev. Lett. 80 (24), 5437–5440.

Shirakawa, T., Honma, S., Honma, K., 2001. Multiple oscillators in the suprachiasmatic nucleus. Chronobiol Int 18, 371–387.

Strogatz, S., 2003. Sync: The Emerging Science of Spontaneous Order. Hyperion, New York, NY.

Tass, P. A., 1999. Phase Resetting in Medicine and Biology. Springer, Berlin and Heidelberg, Germany.

Thain, S. C., Hall, A., Millar, A. J., 2000. Functional independence of circadian clocks that regulate plant gene expression. Curr Biol 10, 951–956.

Ueda, H. R., Hirose, K., Iino, M., 2002. Intercellular coupling mechanism for synchronized and noise-resistant circadian oscillators. J Theor Biol 216, 501–512.

Winfree, A. T., 2001. The Geometry of Biological Time, 2nd Edition. Springer, New York, NY.

Yamaguchi, S., Isejima, H., Matsuo, T., Okura, R., Yagita, K., Kobayashi, M., Okamura, H. 2003. Synchronization of cellular clocks in the suprachiasmatic

nucleus. Science 302: 1408-1412.

Zhou, C., Kurths, J., Hu, B., 2001. Array-enhanced coherence resonance: Nontrivial effects of heterogeneity and spatial independence of noise. Phys. Rev. Lett. 87, 098101.

Zhou, C., Kurths, J. 2002. Spatiotemporal coherence resonance of phase synchronization in weakly coupled chaotic oscillators. Phys. Rev. E 65, 040101.

Tables

Symbol	Definition
ε_i	driving amplitude
$\overline{\varepsilon}$	mean driving amplitude
$\Delta\varepsilon$	driving amplitude spread
ν_i	natural frequencies
$\overline{\nu}$	mean natural frequency
$\Delta\nu$	natural frequency spread
ω_e	external driver frequency
Ω_i	real frequencies
$\overline{\Omega}$	mean real frequency
$\sigma(\Omega_i)$	standard deviation of real frequencies
$P(\Omega_i)$	probability function of real frequencies
η	degree of forced entrainment
$\widehat{R}$	temporal average of mean-field amplitude
ΔR	temporal variation of mean-field amplitude
D	noise intensity
K	coupling strength

Table 1

Definition of used symbols

Figure captions

Fig. 1. Spatial distributions of the driving force ε. *Left*: Uniform random distribution in the interval $[\varepsilon - \Delta\varepsilon, \varepsilon + \Delta\varepsilon]$, with $\overline{\varepsilon} = 0.1$ and $\Delta\varepsilon = 0.05$. *Right*: Gradual distribution according to Eq. (8), with $\overline{\varepsilon}$ and $\Delta\varepsilon$ identical to the left panel.

Fig. 2. Geometrical relation of single-oscillator resonance zones and the driving-parameter space. *Left:* Resonance diagram of a single phase oscillator with natural frequency mismatch ν to an external driver acting with force ε. The shaded triangle marks the phase-locking zone, given by Eq. (9). The line-filled rectangle indicates the situation of a population of uncoupled phase oscillators distributed in $\nu \in [\overline{\nu} - \Delta\nu, \overline{\nu} + \Delta\nu]$ and $\varepsilon \in [\overline{\varepsilon} - \Delta\varepsilon, \overline{\varepsilon} + \Delta\varepsilon]$. *Right:* driving-parameter space $\Delta\varepsilon$ vs. $\overline{\varepsilon}$. The line-filled triangle in the upper left half marks the area given by Eq. (11), which is not explored numerically in this work as it yields mixed positive and negative values of ε_i. The shaded triangle in the lower right corner marks the area given by expression (10), in which the rectangle in the left panel is completely contained in the locking zone, and dominance of the external driver is to be expected.

Fig. 3. Array statistics and observables in the driving-parameter space for four different scenarios, and $\overline{\nu} = 0.02$, $\Delta\nu = 0.05$. The gray scales read, from *top to bottom*: $\overline{\Omega}$, $\sigma(\Omega_i)$, η, $\widehat{R}$, ΔR. The left-most panels (a)-(e) show the values for the uncoupled array, $K = 0$. The center-left column with panels (f)-(k) correspond to a random spatial distribution of ε and global coupling, with $K = 2$. Column (l)-(p) features random distributions of ε, next-neighbour coupling, and $K = 2$. The right-most column (q)-(u) plots the situation of a gradual distributions of ε, next-neighbour coupling, and $K = 2$. The dotted gray lines correspond to Eqs. (10) and (11), compare Fig. 2. The third, additional, dotted line in panels (q)-(u) corresponds to Eq. (12). Solid gray lines mark the passage of the threshold given by Eq. (7). The crosses in the panels for $K = 2$ indicate the location of the special cases exhibited in Fig. 4.

Fig. 4. Special cases of three scenarios without full external synchronization. *Top row:* Contour plots of the spatio-temporal dynamics of three scenarios with partial external synchronization. Gray scales represent $\sin(\phi_i(t))$. *Bottom row:* Contour plots of the real frequency distribution $P(\Omega)$ as a function of coupling strength K. Gray dotted lines mark the values $\Omega = 0$, where $\Omega = \omega_e$, and $\Omega = \overline{\nu} = 0.02$. In all cases $\Delta\nu = 0.05$. (a/d) A random spatial distribution of ε and global coupling, with $\overline{\varepsilon} = 0.015$, $\Delta\varepsilon = 0.01$. (b/e) Random spatial distribution of ε, and next-neighbour coupling, $\overline{\varepsilon} = 0.015$, $\Delta\varepsilon = 0.01$. (c/f) Gradual spatial distribution of ε, and next-neighbour coupling, $\overline{\varepsilon} = 0.06$, $\Delta\varepsilon = 0.05$.

Fig. 5. Proportions of driving-parameter space above thresholds (7) as a function of K. Symbols represent $\diamond : \eta$, $\triangle : \widehat{R}$, $\square : \Delta R$. The minimum of the three criteria, i.e. the proportion of the area with full synchronization, is marked by the bold line. *Top:* Deterministic oscillators, $\overline{\nu} = 0.02$, $\Delta\nu = 0.05$. *Bottom:* Noisy oscillators, $D = 0.01$. (a/d) Random distribution of ε, global coupling, (b/e) random distribution of ε, next-neighbour coupling, (c/f) gradual distribution of ε, next-neighbour coupling.

Fig. 6. Limits of full external synchronization in driving-parameter space. Compared are the case of deterministic oscillators (dotted line) and stochastic oscillators with D=0.01 (solid lines) at $K = 2$, featuring local coupling. *Top:* Random spatial distribution of ε, *bottom:* gradual distribution. All other parameters as in Fig. 3.

Fig. 7. Limits of full entrainment in driving-parameter space for $\overline{\nu} = 0.1$. The solid line marks the border where all conditions (7) are fulfilled. For all other parameters and explanations refer to Fig. 3. In (d) the gray dotted line in addition to the ones given by Eqs. (10) and (11), is defined by Eq. (13).

Figure 1

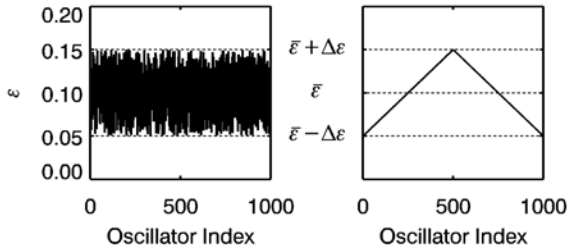

Figure 2

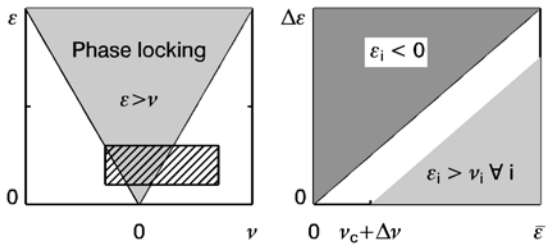

Figure 3

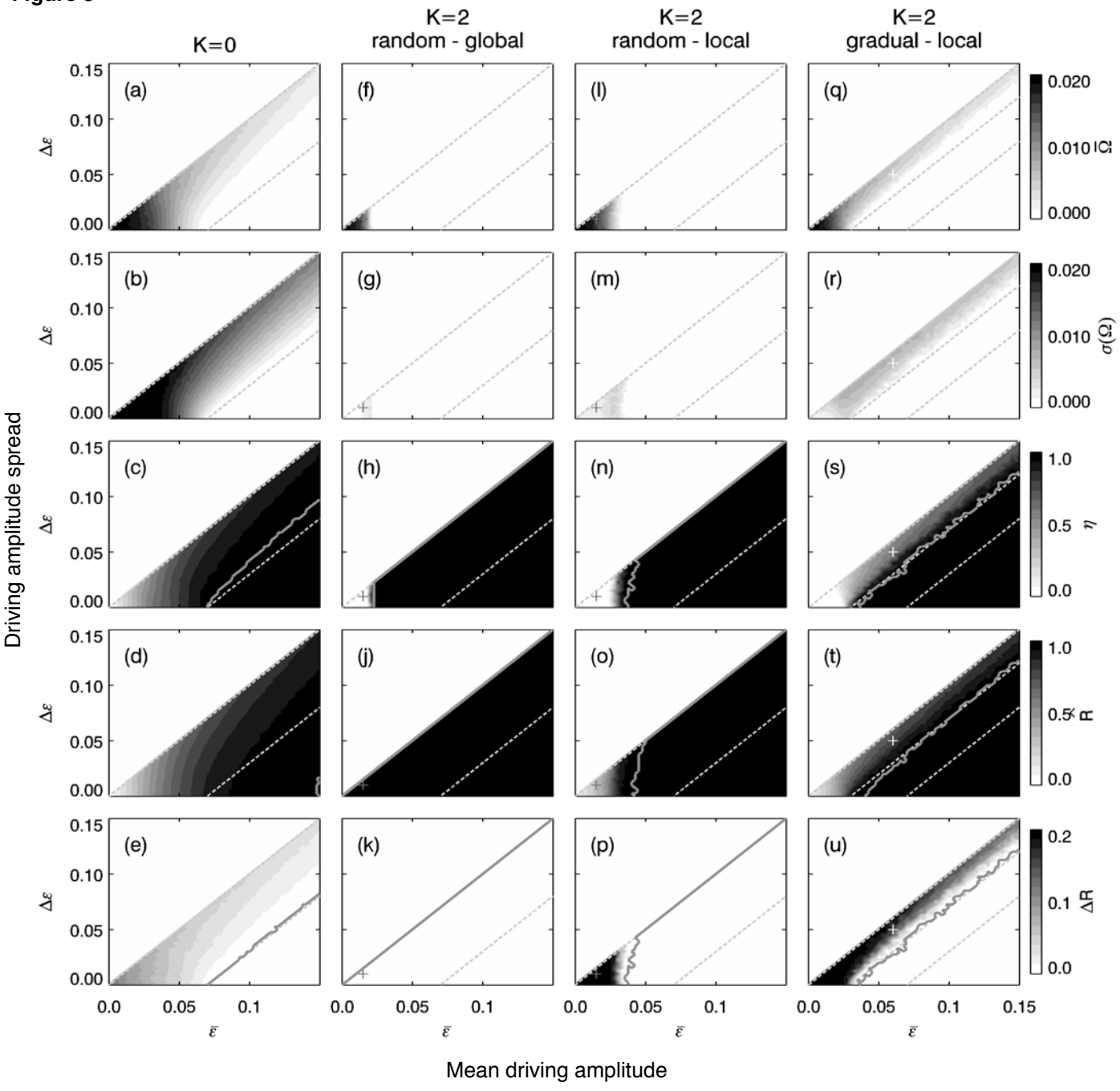

Figure 4

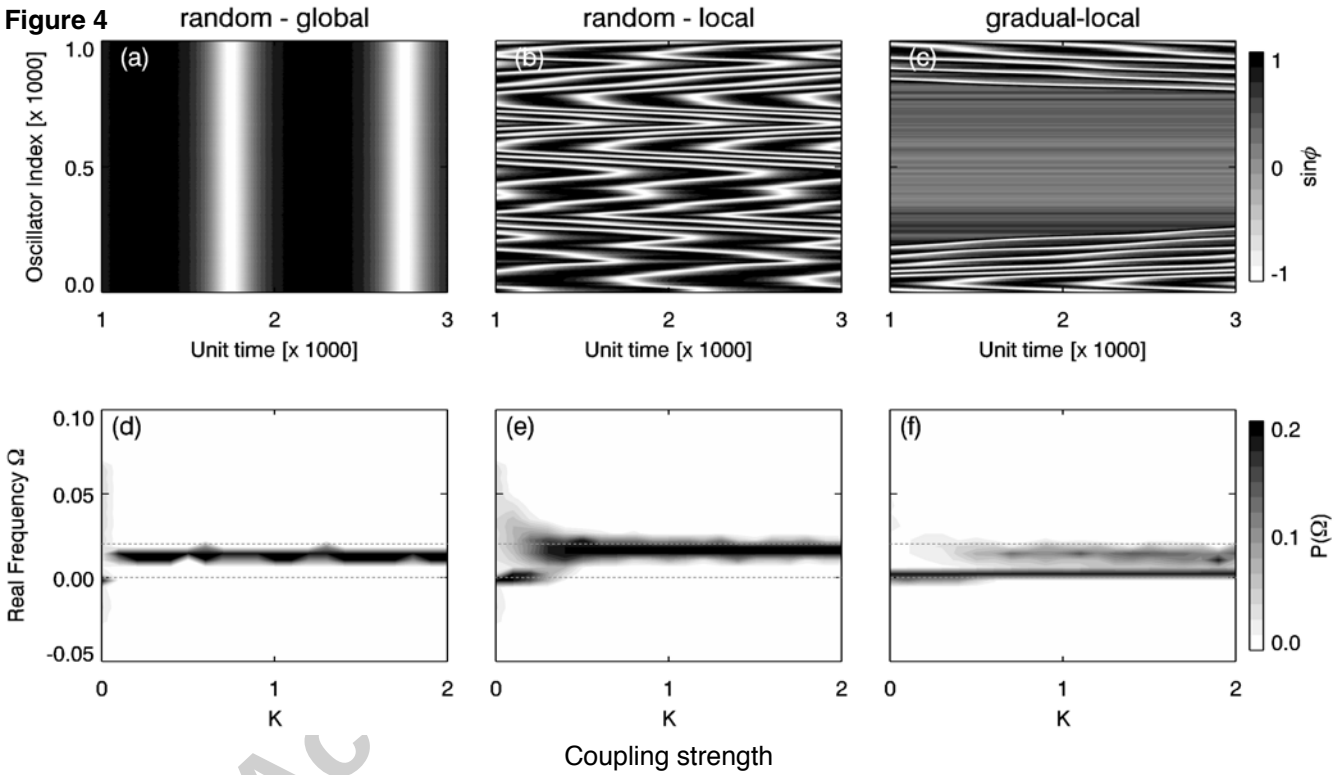

Figure 5

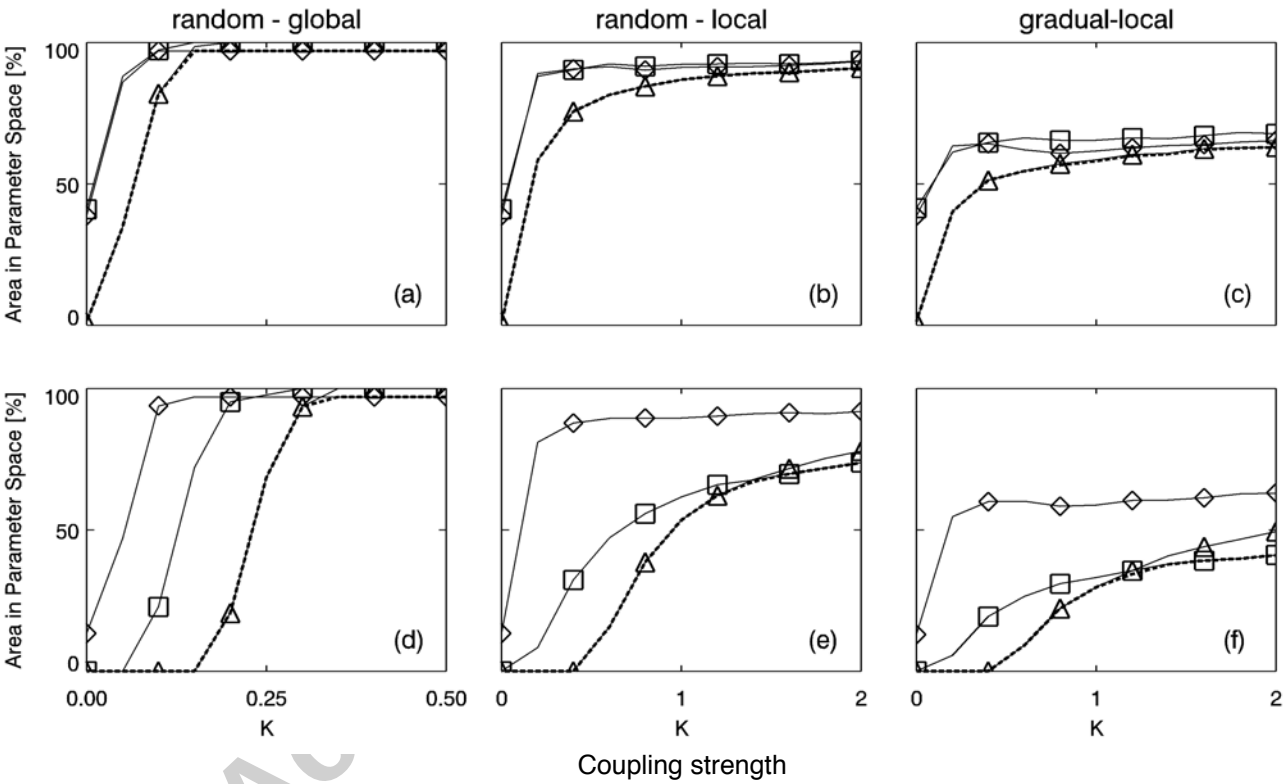

Figure 6

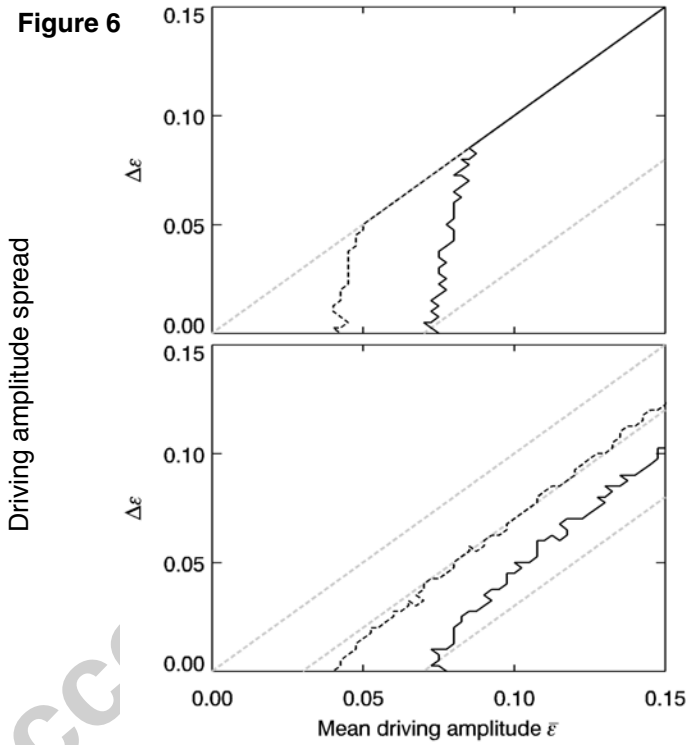

Figure 7